Toward an experimental synthesis of the chondritic insoluble organic matter

Kasia Biron, Sylvie Derenne, François Robert, Jean-Noël Rouzaud

Towards an experimental synthesis of the chondritic insoluble organic matter

Kasia BIRON[a,b,c], Sylvie DERENNE[a,b,*], François ROBERT[c], Jean –Noël ROUZAUD[d]

[a]CNRS, UMR 7619 METIS, F-75005 Paris, France
[b]Sorbonne Universités, UPMC Univ Paris 06, CNRS, EPHE, UMR 7619 METIS, F-75005 Paris, France
[c] IMPMC, CNRS/MNHN UMR 7202, Paris, France
[d]Laboratoire de Géologie, ENS/CNRS UMR 8538, Paris, France
*Corresponding author. E-mail: sylvie.derenne@upmc.fr

Abstract - Based on the statistical model proposed for the molecular structure of the insoluble organic matter (IOM) isolated from the Murchison meteorite, it was recently proposed that, in the solar T-Tauri disk regions where (photo)dissociation of gaseous molecules takes place, aromatics result from the cyclisation/aromatization of short aliphatics. This hypothesis is tested in the present study, with *n*-alkanes being submitted to high frequency discharge at low pressure. The contamination issue was eliminated using deuterated precursor. IOM was formed and studied using solid state nuclear magnetic resonance, pyrolysis coupled to gas chromatography and mass spectrometry, RuO_4 oxidation and high resolution transmission electron microscopy. It exhibits numerous similarities at the molecular level with the hydrocarbon backbone of the natural IOM, reinforcing the idea that the initial precursors of the IOM were originally chains in the gas. Moreover, a fine comparison between the chemical structure of several meteorite IOM suggests either that (i) the meteorite IOMs share a common precursor standing for the synthetic IOM or that (ii) the slight differences between the meteorite IOMs reflect differences in their environment at the time of their formation *i.e.* related to plasma temperature that, in turn, dictates the dissociation/recombination rates of organic fragments.

Keywords: insoluble organic matter, carbonaceous meteorite, irradiation, molecular structure, synthesis.

INTRODUCTION

Carbonaceous meteorites are considered as the most primitive objects of the Solar system and, as such, they contain valuable information regarding its formation. They are fragments broken from asteroids that have remained fairly unprocessed surviving their fall on Earth from space. These objects contain up to 4% of carbon. Most of this carbon occurs as organic matter, which comprises a large diversity of extraterrestrial organic molecules along with macromolecular insoluble organic matter (IOM) (Robert and Epstein, 1982; Cronin and Chang, 1993). The analysis of the chemical composition of the meteoritic organic matter has been mainly focused on the Murchison meteorite over the last three decades. The chemical structure of the IOM was recently investigated using a combination of analytical approaches including various spectroscopic methods (Cronin et al., 1987;

Gardinier et al., 2000; Binet et al., 2002; Cody et al., 2002; Binet et al., 2004; Cody and Alexander, 2005; Orthous-Daunay et al., 2010), thermal and chemical degradations followed by gas chromatography coupled with mass spectrometry (GC-MS), (Studier et al., 1972; Levy et al., 1973; de Vries et al., 1993; Sephton et al., 1998; Sephton, 2004; Remusat et al., 2005a; Remusat et al., 2005b; Sephton, 2013) along with high-resolution transmission electron microscopy (Derenne et al., 2005; Le Guillou et al, 2012).

Taken together, all the data derived from the aforementioned analytical methods led to propose a model of molecular structure for the IOM of Murchison (Derenne and Robert, 2010). This structure, based on small highly substituted aromatic units linked by short but highly branched aliphatic chains suggests a formation pathway in which the aromatic units result from the cyclisation/aromatization of the aliphatic chains. The aim of the present study is to test experimentally this mechanism by synthesizing an analogue to the hydrocarbon skeleton of the meteorite IOM.

Several attempts to synthesize analogues of extraterrestial organic matter have been reported so far. They often aim at reconciling the spectroscopic observations on astrophysical media with those obtained on synthetic organic matter. Various targets were distinguished in the literature such as cometary ices, interstellar organic molecules (on grains or in the gas phase gas), interplanetary dust particles (IDPs), meteorites, or Titan's aerosols. As a result, different experimental devices have been set up. A lot of effort has been put on the irradiation of ice mixtures comprising small molecules (CO, CO_2, CH_3OH, H_2CO, CH_4) that are among the most abundant in the interstellar medium (ISM). In addition, in order to produce more complex molecules likely present in the ISM or in comets (Jenniskens et al., 1993; Bernstein et al., 1997; Schutte, 2002; Dworkin et al., 2004), these syntheses succeeded in releasing amino acids upon hydrolysis (Bernstein et al., 2002; Munoz Caro et al., 2002). Moreover, when a polarized light is used for irradiation, enantiomeric excesses could be measured (Nuevo et al., 2007; Danger et al., 2013; Modica et al., 2014). The other main class of synthesis aimed at identifying the carriers of infrared bands observed in the ISM and these syntheses involve hydrocarbons. Laser pyrolysis of various hydrocarbons (ethylene, acetylene, butadiene and benzene) was shown to produce soluble and insoluble OM, mostly aromatic (Galvez et al., 2002; Jäger et al., 2006) although the formation of aliphatic carbons upon acetylene pyrolysis could be revealed through Fourier transform infrared spectroscopy and ^1H nuclear magnetic resonance (Schnaiter et al., 1999;

Biennier et al., 2009). Combustion of ethylene, acetylene or propylene in O_2 led to the formation of soots (Pino et al., 2008; Carpentier et al, 2013). Photolysis of a plasma of hydrocarbons at low temperature (10 K) resulted in a so-called hydrogenated amorphous carbon polymer exhibiting a strong aliphatic character and considered as a good analogue for the diffuse ISM organic matter (Tokunaga and Wada, 1997; Dartois et al., 2004; Dartois et al., 2005). It must be noted that the aforementioned synthesized materials were further subjected to various treatments (ion or UV irradiation, UV photoprocessing, thermal annealing) to mimic the effects of cosmic rays or the evolution of these materials within molecular clouds or diffuse clouds (Jenniskens et al., 1993; Strazzulla et al., 1995; Goto et al., 2000; Godard et al., 2011). Ice irradiation produced the precursor of amino acids which were also identified upon hydrolysis of meteoritic OM. Irradiation of PAHs in water ice yielded oxidized PAHs similar to some reported in the extracts of meteorites (Bernstein et al., 2002; Ashbourn et al., 2007) but it cannot be excluded that the latter result from aqueous alteration. Recently, Callahan et al. (2013) reported the synthesis of a series of polyphenyl compounds upon benzene irradiation. The same compounds were shown to be present, although in trace amounts, in the organic extract of Murchison meteorite.

As stressed above, the aim of most of these studies was the search for spectroscopic signatures of synthetic materials produced in circumstellar or interstellar conditions. However, as far as the solid phase is concerned, an unique molecular structure can rarely be unambiguously attributed to spectroscopic signatures. In the case of the IOM isolated from meteorites, this issue is circumvented since the combination of various available laboratory techniques gives an access to its chemical structure at the molecular level. In the present study, we used this multiple analytical approach that has already given successful results on natural samples, to reconstruct the molecular structure of the polyaromatic IOM condensed from aliphatic hydrocarbons submitted to a radio frequency plasma discharge. The aim is to search the synthetic route of the meteorite IOM based on its molecular structure (Derenne and Robert, 2010). The experimental conditions can be transposed to the conditions prevailing at the surface of the circumsolar T-Tauri disk, where ion chemistry and photochemistry take place simultaneously (Willacy and Woods, 2009). The thus formed OM was analysed by GC-MS for its soluble part and contamination issues were addressed using a deuterated precursor. The chemical structure of the synthesized IOM was compared with

that of Murchison through pyrolysis coupled with GC-MS, ruthenium tetroxide (RuO_4) oxidation, solid state ^{13}C NMR and HRTEM.

EXPERIMENTAL

Irradiation experiment

Irradiation experiments were performed in a high vacuum glass line equipped with two pressure gauges in order to control the pressure of the gases on the way in and way out of the reaction. The glass line is fitted with molecular and primary pumps on the way out as all the experiments are performed during the constant flow of the gases. The reaction setup, similar to the so-called Nebulotron (Robert et al., 2011), includes a removable U-shaped Pyrex tube where the synthesis takes place. 2 ml of *n*-alkane (pentane or octane, anhydrous, ≥99%, Sigma-Aldrich) is transferred into the vacuum chamber in the form of gas. The irradiation is performed with Evenson cavity (Fehsenfeld et al., 1964) used to excite microwave discharges with 2450 MHz microwave generator (Opthos Instruments). In the absence of refrigeration, the temperature of the reaction, measured on the outer surface of the Pyrex glass, rises up to 72 °C. It must be noted that the nature of the synthesis does not allow measuring the actual temperature of the gas inside the reaction vessel. The pressure during the synthesis is maintained at 3 mbar and the reflected power on the microwave generator is close to 0 watt. Before each experiment, the high vacuum glass line is cleared from any possible contaminants coming from the air and solvents. The entire system is heated to 100°C under the vacuum for several hours to remove water and other trace gases which may adsorb on the surfaces of the chamber. The influence of several parameters was tested: temperature (344 and 322 K), reaction time (30 and 60 min), precursor chain length (pentane and octane) and forced power of the microwave (30 and 60 watts). Total yield of the reaction is calculated by division of the initial mass of the reagent by final mass of the product multiplied by 100.

Sample extraction

The synthesized organic matter is scraped out of the U-shaped Pyrex tube and further extracted with a mixture of dichloromethane and methanol, 2:1, v:v. The extract is separated from the insoluble residue through centrifugation for 30min at 12000rpm. The supernatant is further concentrated using rotary evaporation. The mass balance is achieved

by weighting the reaction tube before and after each experiment and IOM and SOM after their separation. The soluble fraction is analyzed by GC-MS. The insoluble residue is dried under nitrogen and analyzed using Curie point pyrolysis GC-MS and HRTEM techniques. H and C elemental composition were determined at the CNRS Service Central d'Analyse, Vernaison, France.

GC-MS and Curie point pyrolysis GC-MS (Py GC-MS)

The GC-MS device is an Agilent Technologies 6890N gas chromatograph coupled with an Agilent Technologies 5973 Network mass spectrometer. A fused silica capillary column coated with chemically bound Restek RTX-5Si/MS (30 m × 0.25 mm i.d., 0.5 µm film) is used in a GC oven programmed from 50°C to 320°C at 4°C/min with He as carrier gas. The injector temperature is 280°C in spitless mode. The mass spectrometer operated with electron energy 70 eV, ion source temperature 220°C scanning from 40—700 amu at 2.24 scan.s^{-1}.

Pyrolysis is performed using tubular ferromagnetic wires with a Curie temperature of 650°C. The wires are inductively heated using high frequency generator (Pilodist Curie point pyrolyzer) up to Curie temperature in 0.15 s and maintained at this temperature for 10 s. Ca. 4 mg of sample are loaded in each wire. The pyrolysis unit is coupled to the same GC-MS device as described above. The GC oven program includes a first step at 50 °C for 10 min prior to heating to 320 °C at 2°C/min and the MS scan ranges from 35—800 amu at 0.5 scan.s^{-1}. Compound identification is based on mass spectra, GC retention times, and comparison with literature data.

HRTEM

HRTEM was carried out using a Jeol 2011 microscope, operating at 200 kV. When hkl planes are quasi-parallel to the incident electron beam (*i.e.*, under the Bragg angle) and separated by at least 0.14 nm (the resolution of this microscope), fringes appear due to interference between the transmission electron beam and hkl diffracted beams and are representative of the profile of the hkl planes. In the IOM, the profile of the polyaromatics structure can be directly imaged (Rouzaud and Clinard, 2002; Derenne et al., 2005; Le Guillou et al, 2012). The sample was finely crushed into an agate mortar under ethanol. A droplet of the obtained suspension was deposited on a lacey carbon grid and dried. Only

very thin particles (>10 nm if possible) and placed across the web of the lacey grid were imaged, in order to avoid artefacts due to the quasi-amorphous carbon-supporting film.

Image analyses were conducted in a similar way as described by Derenne et al. (2005). In brief, quantitative structural data are obtained after skeletonization of selected HRTEM images (Galvez et al., 2002; Rouzaud and Clinard, 2002; Le Guillou et al., 2012). The image is processed by specific software that reduces the noise background by filtration in the Fourier transform domain. After selecting a threshold, a binary image is obtained and represents a skeleton of carbon layers profile. This skeleton is further analyzed and the length of all the fringes (L, *i.e.* the extent of the aromatic layers) is measured. Coherent domains are defined by the parts of the polyaromatic planes that are involved in the stacking of parallel planes (within a 15° margin). They are characterized by the number N of stacked layers and interlayer spacing d. Two neighbor fringes are considered as single, *i.e.* not stacked when their angle is larger than 15° or their spacing larger than 0.7 nm.

Nuclear magnetic resonance (NMR)

Solid state ^{13}C NMR spectra of synthesized IOM were obtained at 125 MHz (Bruker AV500 spectrometer) using a 4 mm resonance Bruker MAS probe, magic angle spinning at 14kHz, cross-polarization sequence with 3 s recycle time and contact times t_c ranging from 100 µs to 9 ms. Each spectrum was the result of 16000 scans. Free induction decays were analyzed with the Bruker TopSpin program and spectra were decomposed using the Dmfit program (Massiot et al., 2002). The chemical shifts were standardized to the TMS scale (0 ppm) and were adjusted using ^{13}C-labeled adamantane. The assignment of the signals was performed according to (Gardinier et al., 2000).

Fourier transform infrared spectroscopy (FTIR)

The synthesized IOM was mixed with KBr and pressed to form pellets. FTIR spectra were recorded using a Bruker Tensor 27 spectrometer. The spectra (32 scans) were recorded after pellet desiccation at room temperature for 4 hours.

Ruthenium Tetroxide Oxidation (RuO_4 oxidation)

The experimental conditions are based on previously published oxidation of Murchison and Orgueil meteorite IOM (Remusat et al., 2005b). A mixture of 1 mL of CCl_4, 2

Code de champ modifié

mL of distilled water, 1 mL of CH_3CN, 500 mg of sodium metaperiodate (Sigma-Aldrich), and 50 mg of IOM sample were stirred for 30 min at room temperature. Then 5 mg of ruthenium (IV) dioxide (Sigma-Aldrich) were added followed by constant stirring. After 4 h, few drops of isopropanol were added to stop the reaction, then after 5 min the residue was separated by filtration and successively rinsed with 10 ml of MeOH, 20 ml of CH_2Cl_2, and 20 ml of distilled water. The organic filtrates were dried over sodium sulfate. The aqueous filtrate was extracted with distillated ether and combined with the organic filtrates. This organic solution was concentrated by rotary evaporation and dried under N_2 at room temperature prior to silylation which is automatically performed in the GC autosampler by heating up 100 µl of solution with 10 µl N,O-Bis(trimethylsilyl)trifluoroacetamide (BSTFA) for 10 min at 60°C. An aliquot of the organic solution was also methylated by refluxing it into MeOH for 1h in the presence of few drops of acetyl chloride. Silylated ethers and methyl esters were analyzed using GC-MS with the aforementioned experimental conditions. Procedural blank experiments, with and without standard diacids (succinic, glutaric, and adipic acids), were carried out to rule out any laboratory pollution among the oxidation products and check that no short products are lost during the analytical procedure. The oxidation reaction was carried out in 5 replicates.

RESULTS

Synthesis

The total yield of synthesized material ranges from 0.3 to 15 % depending on the synthesis parameters (Table 1). An increase in temperature, power and reaction time as well as the use of octane instead of pentane, *i.e*. the increase in C number of the alkane precursor, result in an increase in the yield. The maximum yield, 15 wt %, is thus obtained after 60 min of irradiation using *n*-octane as a precursor at 60 watts forced power at 72 °C (Table 1). Under these conditions, the soluble and insoluble organic matter is produced in the ratio of 15:85. GC-MS and pyrolysis GC-MS analyses further indicate that the different factors influences the yield of the reaction but do not have any impact on the chemical structure of the synthesized products.

Contamination issue

Before a detailed analysis of the synthesized OM, the contamination had to be addressed. Syntheses performed using deuterated and unlabeled *n*-pentane under the same conditions led to similar results as shown by the two GC-MS traces of the soluble fractions (Fig.1). GC-MS identification shows that all peaks are hydrocarbons and that the trace obtained from the labeled pentane only comprises the deuterated counterparts of the compounds present in the initial trace. Indeed, the difference in molecular weight for each compound equals the number of H in the reference compound. This clearly rules out any contamination and shows that the analyzed products are actually formed from the alkane precursor. A detailed investigation of these products is reported below.

Characterization of the soluble OM by GC-MS

All the identified compounds in the soluble fraction (Fig. 2, Table 2) correspond to polycyclic hydrocarbons with two (1-4,6) to five rings (24-26), the most abundant being phenanthrene (15) and pyrene (21). In addition to the parent compound themselves, some counterparts bearing short alkyl substituents (C_1-C_3) are also identified. The composition of the soluble fraction obtained after octane irradiation shows that the fragmentation of the aliphatic precursor leads to the formation of aromatic compounds, thus supporting the proposed mechanism. In addition, the similarity in chemical composition of the soluble OM formed under various conditions (time, temperature, precursor chain length and forced power of the microwave generator) suggests that the first step in the synthesis involves the breakdown of the precursor into small units. More especially, it must be noted that the increase in yield between the synthesis performed from pentane and octane likely only reflects an increase in the number such units. It has been checked that there is no trace of octane left in the products, indicating that the precursor is completely cleaved in the plasma. More generally, no aliphatic compound could be detected.

Pyrolysis-GC-MS analysis of the IOM

Pyrolysis-GC-MS is commonly used to study macromolecular OM in terrestrial samples like kerogens and coals but also in extraterrestrial samples such as meteorites (Murae, 1995; Komiya and Shimoyama, 1996; Remusat et al., 2005a; Okumura and Mimura, 2011; Sephton, 2013) and tholins (Khare et al., 1981; McGuigan et al., 2006; Szopa et al., 2006). The IOM synthesized in the present study was therefore analyzed using Curie point

pyrolysis. The pyrochromatogram shows a large number of peaks (Fig. 3). Pyrolysis products (Table 3) are aromatic compounds comprising one (1-7, 11, 12) to four rings (29, 30). The abundance of the products seems to decrease with the number of rings suggesting a rather small size for the aromatic units in the macromolecule. Most compounds bear short alkyl substituents (2-7, 10-13, 15-18, 20, 23, 26). A lack of predominance of specific isomers is also observed among all pyrolysis products.

The pyrolysate of the synthesized IOM only comprises cyclic, mainly aromatic products. It cannot be excluded that at least a part of these products underwent cyclization and aromatization upon pyrolysis and thus were not preexisting in the IOM. Such an artifact should be rather limited as the soluble fraction also exhibits a strong aromatic character and that soluble and insoluble fractions are expected to represent a continuum in molecular weight and cross-linking. However, due to limitations in GC-MS, one cannot derive from the aforementioned data an actual distribution of the size of the aromatic units occurring in the synthesized IOM. This can be achieved through HRTEM which provides a direct observation of the polyaromatic units profile and allows semi quantification using image analysis (Rouzaud and Clinard, 2002; Le Guillou et al., 2012;).

HRTEM observation of the IOM

HRTEM images of the synthesized IOM all present rather weak organization of the macromolecules (short and disoriented fringes, large interlayer spacing, very small coherent domains). However, two different types of nanostructure can be distinguished, amorphous-like particles (Fig. 4a, b) and disordered carbon areas characterized by longer fringes (Fig. 4c, d). These two different areas could reflect structural heterogeneity of the sample possibly related to wall effect during the synthesis. Semi-quantitative structural data were obtained after skeletonization of HRTEM images (Rouzaud and Clinard, 2002). The length of all fringes, interlayer spacing and percentage of single layers was individually measured. Average values resulting from hundreds of fringes are reported in the Table 4. They confirm the very small size of the polyaromatic structures as well as their very low level of organization. Indeed, their size ranges between 0.39 and 0.48 nm corresponding to 1 - 4 rings. Most of the layers are not stacked to form coherent domain and can be considered as "single". The mean interlayer spacing is very large, very far from the 0.3354 nm for perfect graphite. The low level of organization observed through HRTEM is consistent with the features highlighted by

GC-MS and Py-GC-MS, the high level of substitution likely preventing the formation of large polyaromatic units as well as their stacking to form coherent domains (a majority of the non-stacked layers is observed even in the less disordered carbon, see Table 4).

NMR analysis of the IOM

All the above-described data were unable to reveal any aliphatic contribution to the IOM, except the short aliphatic substituents of the aromatic pyrolysis products. Similar observations were made on meteoritic IOM despite a significant signal in ^{13}C NMR. Indeed, ^{13}C NMR differentiates the ^{13}C nuclei based on their chemical environments, giving an indication of the overall carbon composition.

Solid state ^{13}C NMR has been applied to numerous types of natural IOM such as coals (Yoshida et al., 2002; Erdenetsogt et al., 2010) and oil shales (Miknis et al., 1979; Maciel and Dennis, 1981; Miknis et al., 1982) but also extraterrestrial samples, like meteorites (Cronin et al., 1987; Gardinier et al., 2000; Cody and Alexander, 2005) or tholins (Derenne et al., 2012). It involves the so-called ^{1}H-^{13}C cross polarization (CP) sequence for sensitivity enhancement and magic angle spinning (MAS) to reduce peak broadening.

The spectrum of the synthesized IOM, recorded with a classical contact time t_c of 3 ms, shows two main peaks assigned to aliphatic and aromatic carbons (Fig.5). The aliphatic peak maximizes at 36 ppm (C in aliphatic chains) and it exhibits two rather well-resolved peaks at around 14 ppm and 23 ppm which reveal the presence of methyl (CH_3) groups which are linked to the aliphatics and aromatics, respectively. The aromatic signal shows a maximum at 127 ppm (mainly protonated aromatic C) along with a shoulder at 138 ppm which can be assigned to non-protonated aromatic C. A spinning side band (SSB) related to the aromatic signal is visible on the left hand side of the spectrum. It must be noted that the second SSB falls under the aliphatic peak. The spectrum can therefore be decomposed into 5 components, namely aliphatic – linked CH_3 at 14 ppm, aromatic – linked CH_3 at 23 ppm, aliphatic C at 35 ppm, protonated aromatic C at 126 ppm and non – protonated aromatic C at 139 ppm along with their SSB (Fig. 5).

In order to acquire quantitative data, 12 spectra were recorded with a contact time t_c ranging from 100 to 9000 μs (Fig. 6a). It must be noted that the smaller peaks and shoulders are hardly visible at the shortest t_c due to inefficient magnetization transfer from H to C. This

reflects either the lack of H on the considered C (139 pm peak) or the molecular motion in the methyl groups (14 and 22 ppm peaks). The evolution of the shape of the spectrum with t_c thus clearly emphasizes the necessity to record spectra at various t_c to derive quantitative data. The latter can be obtained by plotting the intensity I of each signal vs t_c as it is known that, at long t_c, it follows the equation (1),

$$I = I_0 e^{-t_c/T_{1\rho H}} \qquad (1)$$

where I_0 is proportional to the number of C contributing to that signal and $T_{1\rho H}$ is the spin-lattice relaxation time. I_0 can be determined from the intercept in a Ln I = f(t_c) diagram (Fig. 6b). The obtained values for the 5 types of C are gathered in Table 5 and reveal a significant contribution of aliphatic carbons. The latter is confirmed by the presence of bands in the FTIR spectrum (not shown) around 2900 cm^{-1} (aliphatic C-H stretching absorptions) and 1450 and 1375 cm^{-1} (asymmetrical CH_2 and CH_3 and symmetrical CH_3 bending vibrations, respectively) although the spectrum also exhibits bands at 1600 cm^{-1} (C=C in plane vibrations) and between 700 and 900 cm^{-1} (C-H out of plane deformations). Moreover, the relative intensities of the 1450 and 1375 cm^{-1} bands point to a significant contribution of methyl groups in the aliphatic C, in agreement with NMR calculations. However, no molecular information on the aliphatic carbons (chain length, branching level) can be deduced from these spectroscopic data and RuO_4 oxidation had to be performed.

RuO_4 oxidation of the IOM

RuO_4 oxidation is especially efficient in selectively degrading the aromatic rings to CO_2. This mild oxidation results in the release of the acyclic and cyclic aliphatic substituents to which the aromatics are bound as acyclic and cyclic carboxylic acids, the carboxylic functional groups marking the attachment points on the aromatic moieties. Followed by GC/MS identification of the released products, it has been first developed for the analysis of coals (Stock and Tse, 1983; Stock and Wang, 1985; Kidena et al., 2004) and then largely applied on other terrestrial samples like kerogens (Boucher et al., 1990; Standen et al., 1991; Kribii et al., 2001; Li et al., 2004), asphaltenes (Strausz et al., 1999; Li et al., 2010; Muhammad and Abbott, 2013), crude oil (Warton et al., 1999), soil IOM (Quénéa et al., 2005; Winkler et al., 2005) and non-hydrolysable algal biopolymers (Blokker et al., 2000; Blokker et al., 2006). Recently, this technique was also used in the analysis of carbonaceous meteorites (Remusat et al., 2005b).

The oxidation products of the synthesized IOM are analyzed after silylation. They mainly comprise aliphatic mono- and dicarboxylic acids along with small amounts of aromatic acids (Fig. 7, Table 6). Monocarboxylic acids (1-5, 9-11, 14, 20, 21, 23) indicate the presence of alkyl chains linked to an aromatic ring and diacids (7, 16-18, 22, 24-26, 28, 29) reflect an alkyl bridging between two aromatic units. It must be noted that diacids are less abundant than monoacids. The monocarboxylic acids ranged between C_5 (1-5) to C_{10} (23), showing that the chain length of the substituent comprises 4 to 9 carbon atoms. As for the diacids, their total chain length ranges from C_2 to C_9 (maximum C_6) leading to aliphatic linkages up to 7 carbon atoms. It must be noted that no propanedioic acid (C_3) could be detected, likely due to its degradation into CO_2 and formic acid under the experimental conditions as previously suggested by Stock and Wang (1986). Numerous isomers are observed in both mono- and diacids pointing to a high branching level in these aliphatic chains. Two cycloalkane carboxylic acids are detected with C_5 and C_6 rings (6, 15) as well as a series of ω-1 oxocarboxylic acids ranging from C_5 to C_7 (8, 12, 19). The formation of such ketoacids was reported through oxidation of the double bond in substituted cycloalkenes (Coudret et al., 1996; Reiss et al., 1997; Zimmermann et al., 2005). The presence of such structures is consistent with a weak band at 1680 cm^{-1} in the FTIR spectrum. Taken together, these two types of compounds point to the presence of non-aromatic rings in the IOM, consistently with the presence of indane, indene or dihydronaphthtalene derivatives in the IOM pyrolysate. Aromatic acids comprise benzoic acid (13) along with two isomers of benzenedicarboxylic acid (27), which arise from the oxidation of fused benzene rings in polyaromatic units.

To go further in the identification of the IOM oxidation products, they were also analyzed after methylation. The latter revealed the presence of traces of aliphatic (C_6 and C_7) tricarboxylic acids along with two isomers of benzenetricarboxylic acids which could not be detected in the silylated extract.

DISCUSSION - COMPARISON WITH METEORITE IOM AND COSMOCHEMICAL IMPLICATIONS

The purpose of the present work was to test the ability of synthesizing macromolecular material from small aliphatic units under presolar disk conditions corresponding to regions where a massive (photo)dissociation of gaseous molecules took

place. However, it must be noted that we do not address the physical cause of the dissociation (dense UV photon-dominated regions, high velocity shocks, …)

As the present synthesis only involves C and H atoms and no heteroelement whereas the latter substantially contribute to the meteorite IOM, the comparison between the presently synthesized material and the meteorite IOM should be limited to its hydrocarbon skeleton. Both materials exhibit an aromatic character with a chemical structure based on small aromatic units, as directly imaged by HRTEM. Indeed the average length of the aromatic layers in the disordered area of the synthesized material (0.48 nm) is comparable to that previously reported for Murchison and Orgueil IOM (0.55-0.58 nm; Derenne et al., 2005). In both cases, the more frequent structure corresponds to about a length of 2 fused rings (layers of about 4 fused rings if the structure is considered as isometric). Moreover, these values contain important information: (i) the synthesized IOM is not amorphous (i.e. made of randomly distributed carbon atoms) since sub-nanometric fringes are detected and (ii) this synthesized carbonaceous matter is very far from graphite for which graphene layer size is more than 100 nm and such layers are stacked by tens (whereas subnanometric layers of the synthesized IOM are often single, or piled by two units). Finally, it must be noted that in chondrites of petrologic type >3.0, the evolution of the IOM is controlled by the extent of thermal metamorphism. The polyaromatic layers, shorter than 1 nm in petrologic type ≤ 3.0 chondrites, grow up to sizes between 5 and 10 nm in petrologic type >3.6 chondrites, contributing to the increase of the degree of structural order (Le Guillou et al., 2012). Therefore, according to HRTEM, the synthesized IOM appears to be very similar to the pristine meteoritic IOM as found in non-thermally metamorphosed meteorites.

Beside these aromatic units, FTIR and solid state ^{13}C NMR revealed the presence of aliphatic carbons. Using variable contact time experiment in the CP/MAS sequence, a comparison between the relative abundance of aliphatic and aromatic carbons in the meteorite and synthesized IOM can be achieved although it must be restricted to the carbons which do not bear any heteroelement. Quantitative data derived from NMR have been published on a relatively restricted set of carbonaceous chondrites, namely Murchison, Orgueil, EET92042 and Tagish Lake (Gardinier et al., 2000; Cody et al., 2002; Cody and Alexander, 2005). They reveal differences in aromaticity, (*i.e.* the intensity ratio of aromatic to total signal) with the following order of increasing aromaticity, from EET92042 to Orgueil, Murchison and Tagish Lake. This has been interpreted as the result of a progressive trend of

IOM alteration on the parent body, the aromatic units being considered as more refractory than the aliphatic chains. The presently synthesized IOM exhibits a higher aliphatic character than Orgueil, Murchison and Tagish Lake and rather similar to that of EET92042. This is further supported by an H/C elemental ratio of 1.11 for the synthesized IOM, substantially higher than that of the IOM from Orgueil, Murchison and Tagish Lake.

A more precise comparison between meteorite and synthesized IOM can be achieved through Py-GC-MS and RuO_4 oxidation. Indeed, molecular information can be derived from these techniques on aromatic and aliphatic units respectively.

Most of the compounds identified in the pyrolysate of the synthesized material were also reported upon pyrolysis of Murchison and Orgueil (Table 3). Moreover, to achieve quantitative comparison between the extraterrestrial and synthesized samples, the relative abundances were compared. To this end, the peak intensities were normalized to 2-methylnaphthalene, as this compound is the most abundant one in the present pyrolysate, and further compared with those calculated from Murchison and Orgueil pyrolysate (Fig. 8) .A general good agreement is observed as most compounds fall close to the 1:1 line, especially when compared with Orgueil.

As far as we are aware, RuO_4 oxidation was only performed on Orgueil and Murchison meteorites (Remusat et al., 2005b). They mainly released aliphatic di- and tricarboxylic acids, along with benzenecarboxylic acids although in lesser amount. These products are also identified in the present study (Table 6) but with different distribution (Fig. 9). The relative abundance of the diacids increases from C_4 to C_6 and then decreases in the synthesized IOM whereas a regular decrease with the chain length is observed in the meteorites. It must also be noted that the methyl substituted diacids are more abundant than their parent compound (e.g. 17 and 18 with respect to 16) contrary to what was observed in Orgueil and Murchison. Another major difference between these two types of IOM is the presence of the C_5 to C_{10} monocarboxylic acids (Fig. 7, Table 6) which were not observed in the meteorites.

Taken together, the differences in distribution and the presence of monocarboxylic acids are consistent with the higher aliphaticity previously deduced from NMR for the synthesized IOM. The presence of ketoacids and cycloalkanoic acids in the RuO_4 oxidation products and of non-aromatic cyclic products in the pyrolysate of the IOM suggests a substantial contribution of non-aromatic unsaturated and saturated rings in the chemical

structure of the synthesized IOM. The latter were at most present in much lower abundance in the meteorites. As these structures can be considered as intermediates in the aromatization process, it seems that the synthesized IOM has not reached the same aromatization stage as the one observed in Orgueil and Murchison IOM. Two hypotheses can be put forward to account for this difference. (i) Either all the aforementioned meteorites share a common precursor and they further undergo aromatization to different extents, EET92042 being the most pristine; (ii) or they are formed in different regions of the nebula where slightly different conditions prevail especially for dissociation rates and therefore hydrogen content. This second hypothesis is supported by a recent study reporting on the influence of plasma temperature on its composition (Lombardi et al., 2005). In this study, the distribution of the various species in a CH_4/H_2 microwave discharge is determined as a function of temperature, thus showing that the higher plasma temperature, the more atomic hydrogen. Atomic hydrogen being known to prevent the formation of aromatic hydrocarbons, less aromatic material will be formed under conditions that favor high plasma temperature. In this context, EET92042 would be formed in nebula regions where higher dissociation rates take place whereas the more aromatic Tagish Lake would have formed in regions with lower dissociation rates, the synthesis performed in the present study being more representative of the formation of IOM from EET92042.

CONCLUSION

First, it is worth noting that synthesis performed with pentane or octane yields similar compounds. Therefore the precursors of these compounds do not retain the "memory" of the starting material. The carbon number of the reaction products is independent of their precursors and the polymerization yields compounds with molecular weight higher than that of the precursor. In other words, similar resulting organic residues can be obtained from any type of aliphatic hydrocarbons suggesting their cleavage into very small common units. Whether the polymerization takes place within the gas phase or onto the vessel walls remains an open issue.

Aliphatic hydrocarbons submitted to a plasma discharge under reduced pressure yield organic matter among which 85% is insoluble. Solid state ^{13}C NMR shows that the synthesized IOM comprises both aromatic and aliphatic carbons, thus revealing the formation of aromatic moieties from aliphatic units in the gas phase and/or on grains. Py-

GC-MS and HRTEM analyses of the synthesized IOM point to strong similarities at the molecular level with the hydrocarbon skeleton of Orgueil and Murchison IOM. ^{13}C NMR and RuO_4 oxidation confirm these qualitative similarities although suggesting that the structure of the synthesized IOM has not reached the same stage of aromaticity as the meteorite IOM. Based on a comparison performed on IOM from various meteorites, two hypotheses can be put forward to account for this difference: (i) either the synthesized IOM exhibits a pristine chemical structure, which has not undergone any alteration similar to that which takes place on the parent body or (ii) the differences observed between the meteorites reflect differences in their formation conditions, the synthesized IOM being formed in an environment closer to that of EET92042 than Orgueil and Murchison. These differences would mainly rely on plasma temperature and consequently dissociation rates and hydrogen availability. These results and their comparisons with those obtained on the IOM isolated from the meteorites support the proposal according to which aromatics in the IOM meteorites result from the cyclisation/aromatization of aliphatics in the gas.

Acknowledgments - Christelle Anquetil (CNRS METIS) is thanked for her technical support in GC-MS and Py-GC-MS. Financial support is acknowledged from Labex Matisse This work was supported by French state funds managed by the ANR within the Investissements d'Avenir programme under reference ANR-11-IDEX-0004-02, and more specifically within the framework of the Cluster of Excellence MATISSE (PhD grant to K. B.), CNRS-INSU National program of planetology and CNES Exobiology program.

REFERENCES

Ashbourn S.F.M., Elsila J.E., Dworkin J.P., Bernstein M.P., Sandford S.A., and Allamandola L.J. 2007. Ultraviolet photolysis of anthracene in H_2O interstellar ice analogs, Potential connection to meteoritic organics. Meteoritics & Planetary Science 42:2035-2041.

Bernstein M.P., Sandford S.A., and Allamandola L.J. 1997. The infrared spectra of nitriles and related compounds frozen in Ar and H_2O. Astrophysical Journal 476:932-942.

Bernstein M.P., Dworkin J.P., Sandford S.A., and Allamandola L.J. 2002. Ultraviolet irradiation of the polycyclic aromatic hydrocarbon (PAH) naphthalene in H_2O. Implications for meteorites and biogenesis. Advances in Space Research 30:1501-1508.

Biennier L., Georges R., Chandrasekaran V., Rowe B., Bataille T., Jayaram V., Reddy K.P.J., and Arunan E. 2009. Characterization of circumstellar carbonaceous dust analogues produced by pyrolysis of acetylene in a porous graphite reactor. Carbon 47:3295-3305.

Binet L., Gourier D., Derenne S., and Robert F. 2002. Heterogeneous distribution of paramagnetic radicals in insoluble organic matter from the Orgueil and Murchison meteorites. Geochimica et Cosmochimica Acta 66:4177-4186.

Binet L., Gourier D., Derenne S., Robert F., and Ciofini I. 2004. Occurrence of abundant diradicaloid moieties in the insoluble organic matter from the Orgueil and Murchison meteorites, a fingerprint of its extraterrestrial origin? Geochimica et Cosmochimica Acta 68:881-891.

Blokker P., Schouten S., de Leeuw J.W., Damsté J.S.S., and van den Ende H. 2000. A comparative study of fossil and extant algaenans using ruthenium tetroxide degradation. Geochimica et Cosmochimica Acta 64:2055-2065.

Blokker P., van den Ende H., de Leeuw J.W., Versteegh G.J.M., and Sinninghe Damsté J.S. 2006. Chemical fingerprinting of algaenans using RuO4 degradation. Organic Geochemistry 37:871-881.

Boucher R.J., Standen G., Patience R.L., and Eglinton G. 1990. Molecular characterisation of kerogen from the Kimmeridge clay formation by mild selective chemical degradation and solid state 13C-NMR. Organic Geochemistry 16: 951-958.

Callahan M.P., Gerakines P.A., Martin M.G., Peeters Z., and Hudson R.L. 2013. Irradiated benzene ice provides clues to meteoritic organic chemistry. Icarus 226:1201-1209.

Carpentier Y., Feraud G., Dartois E., ROUZAUD J.N., and PINO T. 2013. Nanostructuration of polyaromatic analogues of the carbonaceous dust. European Conference on Laboratory Astrophysics Book Series. EAS Publications Series 58:399-404.

Cody G.D., and Alexander C.M.O.D. 2005. NMR studies of chemical structural variation of insoluble organic matter from different carbonaceous chondrite groups. Geochimica et Cosmochimica Acta 69:1085-1097.

Cody G.D., Alexander C.M.O.D., and Tera F. 2002. Solid-state (^{1}H and ^{13}C) nuclear magnetic resonance spectroscopy of insoluble organic residue in the Murchison meteorite, a self-consistent quantitative analysis. Geochimica et Cosmochimica Acta 66:1851-1865.

Coudret J.L., Zöllner S., Ravoo B.J., Malara L., Hanisch C., Dörre K., de Meijere A., and Waegell B. 1996. Role of cyclopropanes as activating groups during oxidation reactions with RuO4 generated in situ. Tetrahedron Letters 37:2425-2428.

Cronin J., and Chang S. 1993. Organic Matter in Meteorites, Molecular and Isotopic Analyses of the Murchison Meteorite. In The Chemistry of Life's Origins, edited by. Greenberg J.M., Mendoza-Gómez C.X. and Pirronelle V. Dordrecht, The Netherlands:Kluwer Academic Publishers. pp. 209-258.

Cronin J.R., Pizzarello S., and Frye J.S. 1987. ^{13}C NMR spectroscopy of the insoluble carbon of carbonaceous chondrites. Geochimica et Cosmochimica Acta 51:299-303.

Danger G., Orthous-Daunay F.R., de Marcellus P., Modica P., Vuitton V., Duvernay F., Flandinet L., d'Hendecourt L., Thissen R., and Chiavassa T. 2013. Characterization of laboratory analogs of interstellar/cometary organic residues using very high resolution mass spectrometry. Geochimica et Cosmochimica Acta 118:184-201.

Dartois E., Munoz Caro G.M., Deboffle D., and d'Hendecourt L. 2004. Diffuse interstellar medium organic polymers. Astronomy &Astrophysics 423:33-36.

Dartois E., Munoz Caro G.M., Deboffle D., Montagnac G., and d'Hendecourt L. 2005. Ultraviolet photoproduction of ISM dust. Astronomy &Astrophysics 432:895-908.

de Vries M.S., Reihs K., Wendt H.R., Golden W.G., Hunziker H.E., Fleming R., Peterson E., and Chang S. 1993. A search for C_{60} in carbonaceous chondrites. Geochimica et Cosmochimica Acta 57:933-938.

Derenne S., Coelho C., Anquetil C., Szopa C., Rahman A.S., McMillan P.F., Corà F., Pickard C.J., Quirico E., and Bonhomme C. 2012. New insights into the structure and chemistry of Titan's tholins via ^{13}C and ^{15}N solid state nuclear magnetic resonance spectroscopy. Icarus 221:844-853.

Derenne S., and Robert F. 2010. Model of molecular structure of the insoluble organic matter isolated from Murchison meteorite. Meteoritics & Planetary Science 45:1461-1475.

Derenne S., Rouzaud J.-N., Clinard C., and Robert F. 2005. Size discontinuity between interstellar and chondritic aromatic structures, A high-resolution transmission electron microscopy study. Geochimica et Cosmochimica Acta 69:3911-3917.

Dworkin J. P., Gillette J. S., Bernstein M. P., Sandford S.A., Allamandola L. J., Elsila J. E., McGlothlin D. R., and Zare R.N. 2004. An evolutionary connection between interstellar ices and IDPs? Clues from mass spectroscopy measurements of laboratory simulations. Advances in Space Research 33:67-71.

Erdenetsogt B.-O., Lee I., Lee S.K., Ko Y.-J.,and Bat-Erdene D. 2010. Solid-state C-13 CP/MAS NMR study of Baganuur coal, Mongolia, Oxygen-loss during coalification from lignite to subbituminous rank. International Journal of Coal Geology 82:37-44.

Fehsenfeld F. C., Evenson K.M., and Broida H. P. 1964. Microwave discharge cavities operating at 2450 MHz. The review of scientific instruments 36:294-298.

Galvez A., Herlin-Boime N., Reynaud C., Clinard C., and Rouzaud J.-N. 2002. Carbon nanoparticles from laser pyrolysis. Carbon 40:2775-2789.

Gardinier A., Derenne S., Robert F., Behar F., Largeau C., and Maquet J. 2000. Solid state CP/MAS ^{13}C NMR of the insoluble organic matter of the Orgueil and Murchison meteorites, quantitative study. Earth and Planetary Science Letters 184:9-21.

Godard M., Feraud G., Chabot M., Carpentier Y., Pino T., Brunetto R., Duprat J., Engrand C., Bréchignac P., d'Hendecourt L., and Dartois E. 2011. Ion irradiation of carbonaceous interstellar analogues. Astronomy &Astrophysics 529:A146.

Goto M., Maihara T., Terada H., Kaito C., Kimura S., and Wada S. 2000. Infrared spectral sequence of quenched carbonaceous composite subjected to thermal annealing. Astronomy and Astrophysics Supplement Series 141:149-156.

Jäger C., Krasnokutski S., Staicu A., Huisken F., Mutschke H., Henning T., Poppitz W., and Voicu I. 2006. Identification and Spectral Properties of Polycyclic Aromatic Hydrocarbons in Carbonaceous Soot Produced by Laser Pyrolysis. The Astrophysical Journal Supplement Series 166:557-566.

Jenniskens P., Baratta G.A., Kouchi A., de Groot M. S., Greenberg J. M., and Strazzulla G. 1993. Carbon dust formation on interstellar grains. Astronomy and Astrophysics 273:583-600.

Khare B.N., Sagan C., Zumberge J.E., Sklarew D.S., and Nagy B. 1981. Organic solids produced by electrical discharge in reducing atmospheres, Tholin molecular analysis. Icarus 48:290-297.

Kidena K., Matsumoto K., Murata S., and Nomura M. 2004. Nuclear Magnetic Resonance and Ruthenium Ion Catalyzed Oxidation Reaction Analysis for Further Development of Aromatic Ring Size through the Heat Treatment of Coking Coals at >500 °C. Energy and Fuels 18 : 1709–1715.

Komiya M., and Shimoyama A. 1996. Organic compounds from insoluble organic matter isolated from the Murchison carbonaceous chondrite by heating experiments. Bulletin of the Chemical Society of Japan 69:53-58.

Kribii A., Lemée L., Chaouch A., and Amblès A. 2001. Structural study of the Moroccan Timahdit (Y-layer) oil shale kerogen using chemical degradations. Fuel 80 :681-691.

Le Guillou C., Rouzaud J.-N., Bonal L., Quirico E., Derenne S., and Remusat L. 2012. High resolution TEM of chondritic carbonaceous matter, Metamorphic evolution and heterogeneity. Meteoritics & Planetary Science 47:345-362.

Levy R.L., Grayson M.A., and Wolf C.J. 1973. The organic analysis of the murchison meteorite. Geochimica et Cosmochimica Acta 37:467-483.

Li C., Peng P., Sheng G., and Fu J. 2004. A study of a 1.2 Ga kerogen using Ru ion-catalyzed oxidation and pyrolysis–gas chromatography–mass spectrometry, structural features and possible source. Organic Geochemistry 35:531-541.

Li Y., Xiong Y., Liang Q., Fang C., and Wang C. 2010. Application of headspace single-drop microextraction coupled with gas chromatography for the determination of short-chain fatty acids in RuO_4 oxidation products of asphaltenes. Journal of Chromatography 1217:3561-3566.

Lombardi G., Hassouni K., Stancu G.-D., Mechold L., Röpcke J., and Gicquel A. 2005. Modeling of microwave discharges of H_2 admixed with CH_4 for diamond deposition. Journal of Applied Physics 98:053303-1-12.

Maciel G.E., and Dennis L.W. 1981. Comparison of oil shales and kerogen concentrates by ^{13}C nuclear magnetic resonance. Organic Geochemistry 3:105-109.

Massiot D., Fayon F., Capron M., King I., Le Calvé S., Alonso B., Durand J.O., Bujoli B., Gan Z., and Hoatson G. 2002. Modelling one and two-dimensional solid-state NMR spectra. Magn. Reson. Chem. 40:70-76.

McGuigan M., Waite J.H., Imanaka H., and Sacks R.D. 2006. Analysis of Titan tholin pyrolysis products by comprehensive two-dimensional gas chromatography–time-of-flight mass spectrometry. Journal of Chromatography 1132:280-288.

Miknis F.P., Maciel G.E., and Bartuska V.J. 1979. Cross polarization magic-angle spinning 13C NMR spectra of oil shales. Organic Geochemistry 1:169-176.

Miknis F.P., Szeverenyi N.M., and Maciel G.E. 1982. Characterization of the residual carbon in retorted oil shale by solid-state 13C n.m.r. Fuel 61:341-345.

Modica P., Meinert C., de Marcellus P., Nahon, L., Meierhenrich, U.J., and d'Hendecourt, L.L. 2014. Enantiomeric excesses induced in amino acids by ultraviolet circularly polarized light irradiation of extraterrestrial ice analogs: a possible source of asymmetry for prebiotic chemistry. Astrophysical Journal 788:79

Muhammad A .B., and Abbott G.D. 2013. The thermal evolution of asphaltene-bound biomarkers from coals of different rank, A potential information resource during coal biodegradation. International Journal of Coal Geology 107:90-95.

Munoz Caro G.M., Meierhenrich U.J., Schutte W.A., Barbier B., Arcones Segovia A., Rosenbauer H., Thiemann W.H.P., Brack A., and Greenberg J.M. 2002. Amino acids from ultraviolet irradiation of interstellar ice analogues. Nature 416:403-406.

Murae T. 1995. Characterization of extraterrestrial high-molecular-weight organic matter by pyrolysis-gas chromatography/mass spectrometry. Journal of Analytical and Applied Pyrolysis 32:65-73.

Nuevo M., Meierhenrich U.J., d'Hendecourt L., Muñoz Caro G.M., Dartois E., Deboffle D., Thiemann W.H.P., Bredehöft J.H., and Nahon L. 2007. Enantiomeric separation of complex organic molecules produced from irradiation of interstellar/circumstellar ice analogs. Advances in Space Research 39:400-404.

Okumura F,. and Mimura K. 2011. Gradual and stepwise pyrolyses of insoluble organic matter from the Murchison meteorite revealing chemical structure and isotopic distribution. Geochimica et Cosmochimica Acta 75:7063-7080.

Orthous-Daunay F.R., Quirico E., Lemelle L., Beck P., de Andrade V., Simionovici A., and Derenne S. 2010. Speciation of sulfur in the insoluble organic matter from carbonaceous chondrites by XANES spectroscopy. Earth and Planetary Science Letters 300:321-328.

Pino T., Dartois E., Cao A.-T., Carpentier Y., Chamaillé T., Vasquez R., Jones A., P., d'Hendecourt L., and Bréchignac P. 2008. The 6.2 µm band position in laboratory and astrophysical spectra, a tracer of the aliphatic to aromatic evolution of interstellar carbonaceous dust. Astronomy &Astrophysics 490:665-672.

Quénéa K., Derenne S., Gonzalez-Vila F.J., Mariotti A., Rouzaud J.-N., and Largeau C. 2005. Study of the composition of the macromolecular refractory fraction from an acidic sandy forest soil (Landes de Gascogne, France) using chemical degradation and electron microscopy. Organic Geochemistry 36:1151-1162.

Reiss C., Blanc P., Trendel J.M., and Albrecht P. 1997. Novel hopanoid derivatives released by oxidation of Messel shale kerogen. Tetrahedron 53:5767-5774.

Remusat L., Derenne S., Robert F., and Knicker H. 2005a. New pyrolytic and spectroscopic data on Orgueil and Murchison insoluble organic matter, A different origin than soluble? Geochimica et Cosmochimica Acta 69:3919-3932.

Remusat L., Derenne S., and Robert F. 2005b. New insight on aliphatic linkages in the macromolecular organic fraction of Orgueil and Murchison meteorites through ruthenium tetroxide oxidation. Geochimica et Cosmochimica Acta 69:4377-4386.

Robert F., and Epstein S. 1982. The concentration and isotopic composition of hydrogen, carbon and nitrogen in carbonaceous meteorites. Geochimica et Cosmochimica Acta 46:81-95.

Robert F., Derenne S., Thomen A., Anquetil C., and Hassouni K. 2011. Deuterium exchange rate between and organic CH bonds, Implication for D enrichment in meteoritic IOM. Geochimica et Cosmochimica Acta 75:7522-7532.

Rouzaud J.-N., and Clinard C. 2002. Quantitative high-resolution transmission electron microscopy, a promising tool for carbon materials characterization. Fuel Processing Technology 77–78:229-235.

Schnaiter M., Henning T., Mutschke H., Kohn B., Ehbrecht M., and Huisken F. 1999. Infrared Spectroscopy of Nano-sized Carbon Grains Produced by Laser Pyrolysis of Acetylene, Analog Materials for Interstellar Grains. The Astrophysical Journal 519:687-696.

Schutte W.A. 2002. Production of organic molecules in interstellar ices. Advances in Space Research 30:1409-1417.

Sephton M.A. 2004. Organic matter in ancient meteorites. Astronomy & Geophysics 45:08-14.

Sephton M.A. 2013. Aromatic units from the macromolecular material in meteorites, Molecular probes of cosmic environments. Geochimica et Cosmochimica Acta 107:231-241.

Sephton M., Pillinger C., and Gilmour I. 1998. Small-scale hydrous pyrolysis of macromolecular material in meteorites. Planetary and Space Science 47:181-187.

Standen G., Boucher R.J., Rafalska-Bloch J., and Eglinton G. 1991. Ruthenium tetroxide oxidation of natural organic macromolecules, Messel kerogen. Chemical Geology 91:297-313.

Stock L.M., and Tse K.-T. 1983. Ruthenium tetroxide catalysed oxidation of illinois no.6 coal and some representative hydrocarbons. Fuel 62:974-976.

Stock L.M., and Wang S.-H. 1985. Ruthenium tetroxide catalysed oxidation of Illinois No. 6 coal, The formation of volatile monocarboxylic acids. Fuel 64:1713-1717.

Stock L. M., and Wang S.-H. 1986. Ruthenium tetroxide catalysed oxidation of coals: The formation of aliphatic and benzene carboxylic acids. Fuel 35: 1552–1562.

Strausz O.P., Mojelsky T.W.,Faraji F., and Lown E.M. 1999. Additional Structural Details on Athabasca Asphaltene and Their Ramifications. Energy & Fuels 13:207-227.

Strazzulla G., Arena M., Baratta G.A., Castorina C.A., Celi G., Leto G., Palumbo M.E., and Spinella F. 1995. Radiation chemistry of ices of planetological interest at low temperature. Advances in Space Research 16:61-71.

Studier H., Hayatsu M., and Anders E. R., 1972. Origin of organic matter in early solar system—V. Further studies of meteoritic hydrocarbons and a discussion of their origin. Geochimica et Cosmochimica Acta 36:189-215.

Szopa C., Cernogora G., Boufendi L., Correia J.J., and Coll P. 2006. PAMPRE, A dusty plasma experiment for Titan's tholins production and study. Planetary and Space Science 54:394-404.

Tokunaga A. T., and Wada S. 1997. Quenched Carbonaceous Composite, A laboratory analog for carbonaceous material in the interstellar medium. Advances in Space Research 19:1009-1017.

Warton B., Alexander R., and Kagi R.I. 1999. Characterisation of the ruthenium tetroxide oxidation products from the aromatic unresolved complex mixture of a biodegraded crude oil. Organic Geochemistry 30:1255-1272.

Willacy K., and Woods P.M. 2009. Deuterium Chemistry in Protoplanetary Disks. The Astrophysical Journal Supplement Series 703:479-499.

Winkler A., Haumaier L., and Zech W. 2005. Insoluble alkyl carbon components in soils derive mainly from cutin and suberin. Organic Geochemistry 36:519-529.

Yoshida T., Sasaki M., Ikeda K., Mochizuki M., Nogami Y., and Inokuch K. 2002. Prediction of coal liquefaction reactivity by solid state ^{13}C NMR spectral data. Fuel 81:1533-1539.

Zimmermann F., Meux E., Mieloszynski J.-L., Lecuire J.-M., and Oget N. 2005. Ruthenium catalysed oxidation without CCl4 of oleic acid, other monoenic fatty acids and alkenes. Tetrahedron Letters 46:3201-3203.

Table 1. Influence of the various parameters on the yield of synthesized OM.

Alkane	**Temperature (°C)***	**Power (watt)**	**Reaction time (min)**	**Total yield (%)**
n-pentane	72	30	30	0.3
n-pentane	50	60	30	3.9
n-pentane	72	60	30	5.3
n-pentane	72	60	60	6.8
n-octane	72	60	30	10.1
n-octane	72	60	60	15.3

* - temperature of the glass surface of the reaction tube.

Table 2. List of GC-MS identified compounds in the soluble OM synthesized from *n*-octane.

Number	**Compound**
1	Naphthalene
2	2-methylnaphthalene
3	1-methylnaphthalene
4	1-ethylnaphthalene
5	Biphenylene
6	Biphenyl
7	Acenaphthylene
8	Acenaphthene
9	C_3-alkylnaphtalene
10	Phenalene
11	Fluorene
12	9-methylfluorene
13	2-methylfluorene
14	1-methylfluorene
15	Phenanthrene
16	Anthracene
17	2-methylphenanthrene
18	1-methylphenanthrene
19	Cyclopentaphenanthrene
20	Fluoranthene
21	Pyrene
22	Benzofluorenes
23	Methylpyrenes
24	Benzofluoranthene
25	Cyclopentapyrene
26	Dihydrocyclopentapyrene

Table 3. List of identified compounds released upon 650°C pyrolysis of the synthesized IOM and of Murchison and Orgueil meteorites.

Number	Compound		
	Synthesized IOM	Murchison*	Orgueil*
1	Toluene	+	+
2	trimethylcyclopentadiene	-	-
3	Ethylbenzene	+	+
4	1,4- dimethylbenzene	+	+
5	1,3- dimethylbenzene	+	+
6	1,2-dimethylbenzene	-	-
7	C3-alkylbenzenes	+	+
8	Indane	+	-
9	Indene	+	+
10	C4-alkylcyclohexadiene	-	-
11	C4-alkylbenzene	+	+
12	C5-alkylbenzene	-	-
13	Methylindenes	+	+
14	Naphthalene	+	+
15	C2-alkylindanes	-	-
16	Methyldihydronaphthalene	-	-
17	2-methylnaphthalene	+	+
18	1-methylnaphthalene	+	+
19	Biphenyl	+	+
20	C2-alkylnaphtalenes	+	+
21	Acenaphthylene	+	+
22	Acenaphthene	+	+
23	C3-alkylnaphtalenes	+	+
24	Phenalene	+	+
25	Fluorene	+	+
26	C2-alkylbiphenyl	-	-
27	Phenantrene	+	+
28	Anthracene	+	+

29	Fluoranthene	+	+
30	Pyrene	+	+

* based on Remusat et al. (2005a).

Table 4. Average structural parameters of the aromatic units in the synthesized IOM.

	L - average length [nm]	single layer %	d - interlayer spacing [nm]
Amorphous-like carbon	0.39	84	0.41
Disordered carbon	0.48	69	0.39

Table 5 Relative abundances of the different types of C calculated from the CP/MAS ^{13}C NMR spectra in the synthesized IOM.

Carbon type	**δ (ppm)**	**relative abundances (%)**	**Total (%)**
Ali-linked CH_3	14	8	
Aro-linked CH_3	23	6	52
CH_2	35	38	
protonated aromatic C	126	29.5	48
non-protonated aromatic C	139	18.5	

Table 6. Compounds identified through oxidation of synthesized insoluble organic matter.

Number	Compound		
	Synthesized IOM	Murchison	Orgueil
1	isomers of pentanoic acid	-	-
2	n-pentanoic acid	-	-
3	isomers of hexanoic acid	-	-
4	n-hexanoic acid	-	-
5	isomers of heptanoic acid	-	-
6	cyclopentanecarboxylic acid	-	-
7	ethanedioic acid	+	+
8	4-oxopentanoic acid	-	-
9	isomers of octanoic acid	-	-
10	n-heptanoic acid	-	-
11	isomers of nonanoic acid	-	-
12	5-oxohexanoic acid	-	-
13	benzoic acid	+	+
14	n-octanoic acid	-	-
15	cyclohexanecarboxylic acid	-	-
16	butanedioic acid	+	+
17	isomers of pentanedioic acid	+	+
18	isomers of hexanedioic acid	+	+
19	6-oxoheptanoic acid	-	-
20	isomers of decanoic acid	-	-
21	n-nonanoic acid	-	-
22	pentanedioic acid	+	+
23	n-decanoic acid	-	-
24	isomers of heptanedioic acid	+	+
25	hexanedioic acid	+	+
26	heptanedioic acid	-	+
27	benzenedicarboxylic acid	+	+
28	octanedioic acid	-	+

29	nonanedioic acid	-	+

* based on Remusat et al. (2005b)

Fig.1. GC-MS traces of soluble organic matter produced from a) n-pentane, b) fully deuterated n-pentane.

Fig. 2. GC-MS trace of the soluble OM synthesized from n-octane. Numbers refer to Table 2.

Fig. 3. Total ion current (TIC) of the 650°C pyrolysate of synthesized IOM from octane. Numbers refer to Table 3.

Fig. 4. High resolution transmission electron microscopy observation of insoluble organic matter obtained in the laboratory a) and c) raw images and b) and d) corresponding skeletonized images. Raw images obtained with a 500000x magnification (square size : 14 nm x 14 nm).

Fig. 5. Decomposition of the solid state ^{13}C NMR spectrum of the synthesized IOM.

Fig. 6. Solid state ^{13}C NMR spectra of the synthesized product recorded at various contact time (a) and evolution of the intensities with contact time (b).

Fig. 7. TIC of RuO_4 oxidation products of the IOM. The acids are detected as their trimethylsilyl esters.

Fig. 8. Relationship between relative abundances of pyrolysis products (normalized to 2-methylnaphthalene) from Murchison (a) or Orgueil (b) IOM and synthesized IOM (meteorite data from Remusat et al. (2005a). Numbers refer to Table 3.

Fig. 9. Bar diagram comparing the relative abundance of RuO4 oxidation products in the synthesized (light grey) and meteorite (Orgueil in grey and Murchison in black) IOM (meteorite data from Remusat et al. (2005b). Numbers refer to Table 6 and isomers of 18 have been distinguished for a better comparison with meteorite data.

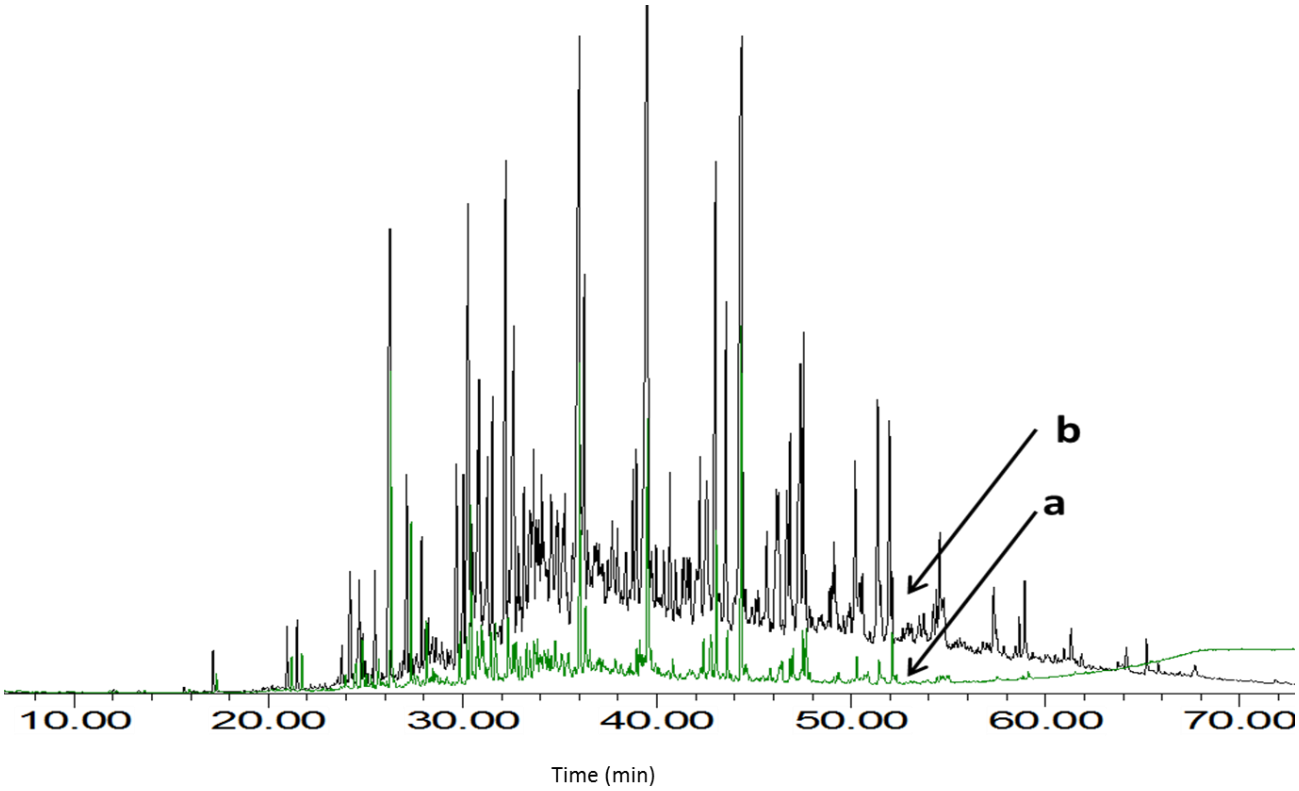

Fig. 1

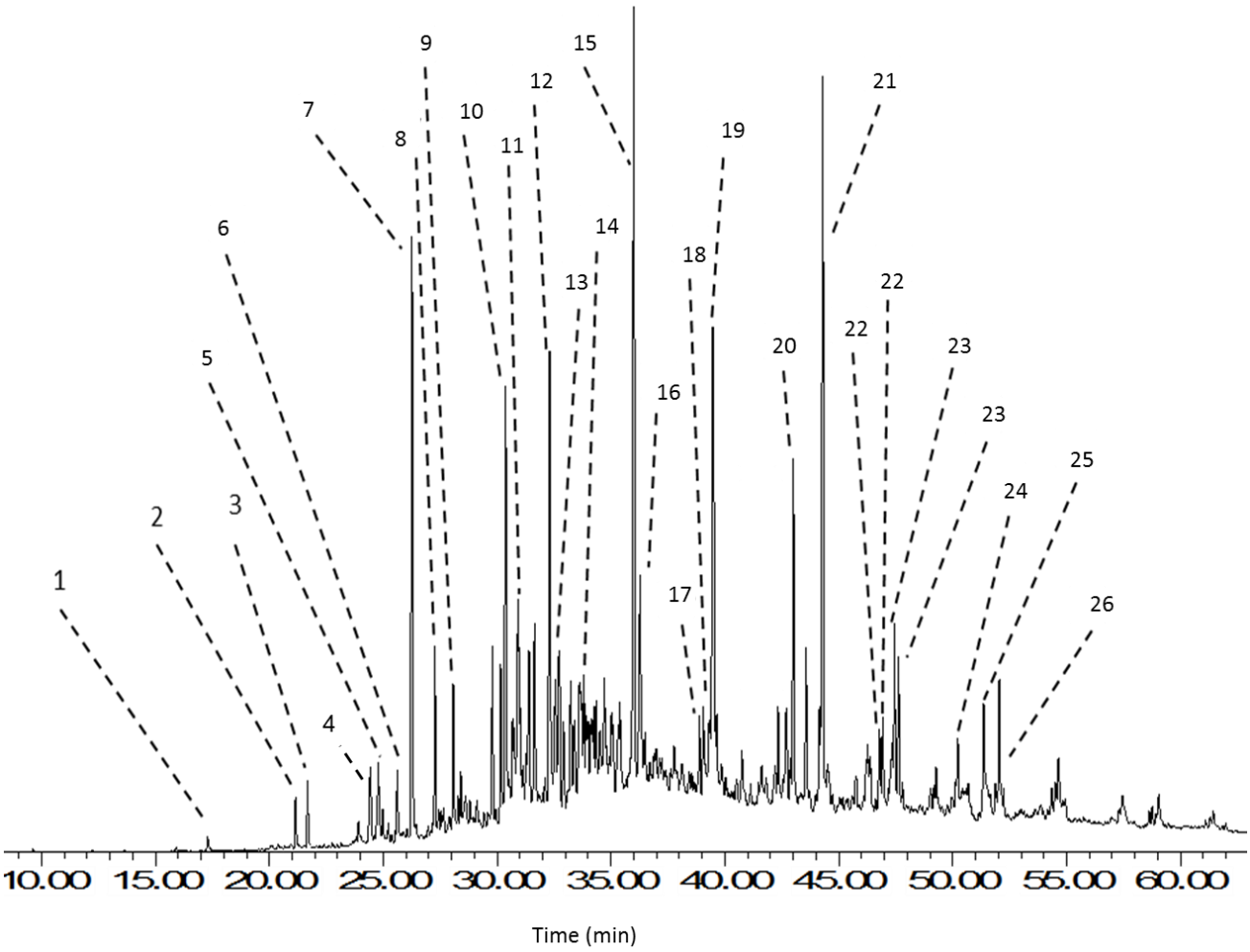
1
2
3
4
5
6
7
8
9
10
11
12
13
14
15
16
17
18
19
20
21
22
22
23
23
24
25
26
10.00
15.00
20.00
25.00
30.00
35.00
40.00
45.00
50.00
55.00
60.00
Time (min)

Fig. 2

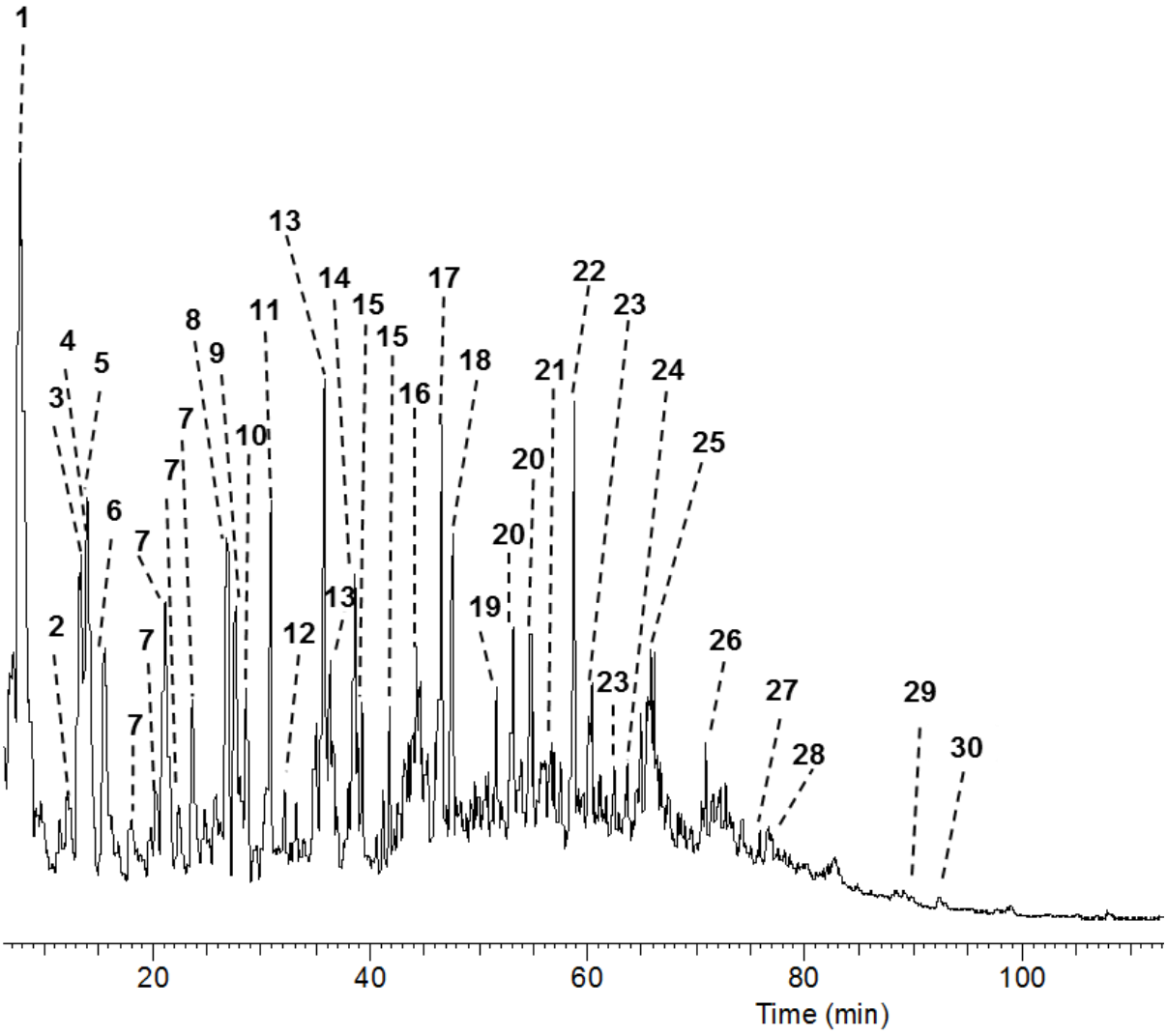
1
2
3
4
5
6
7
7
7
7
7
8
9
10
11
12
13
13
14
15
15
16
17
18
19
20
20
21
22
23
23
24
25
26
27
28
29
30
20
40
60
80
100
Time (min)

Fig. 3

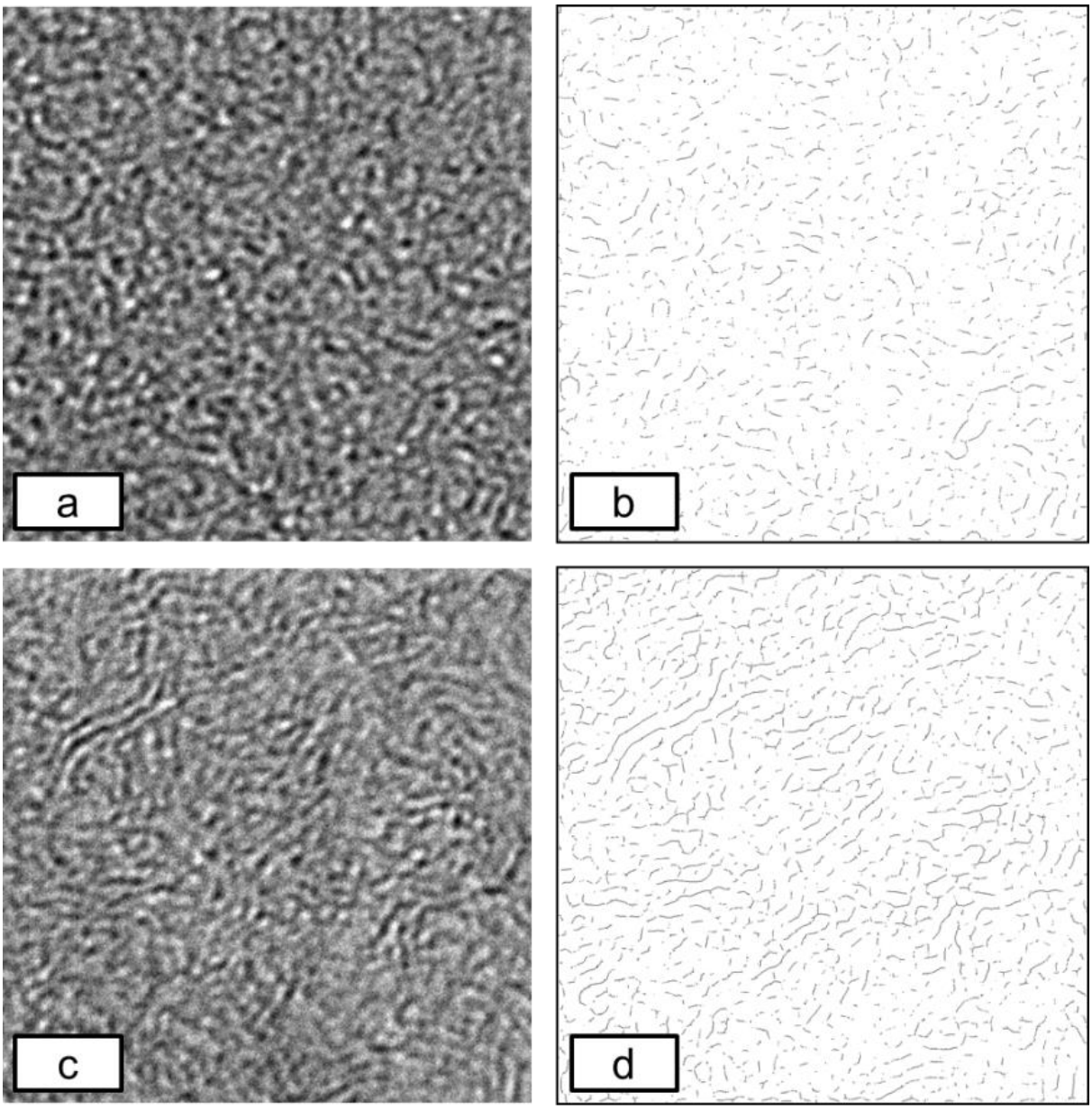

Fig. 4

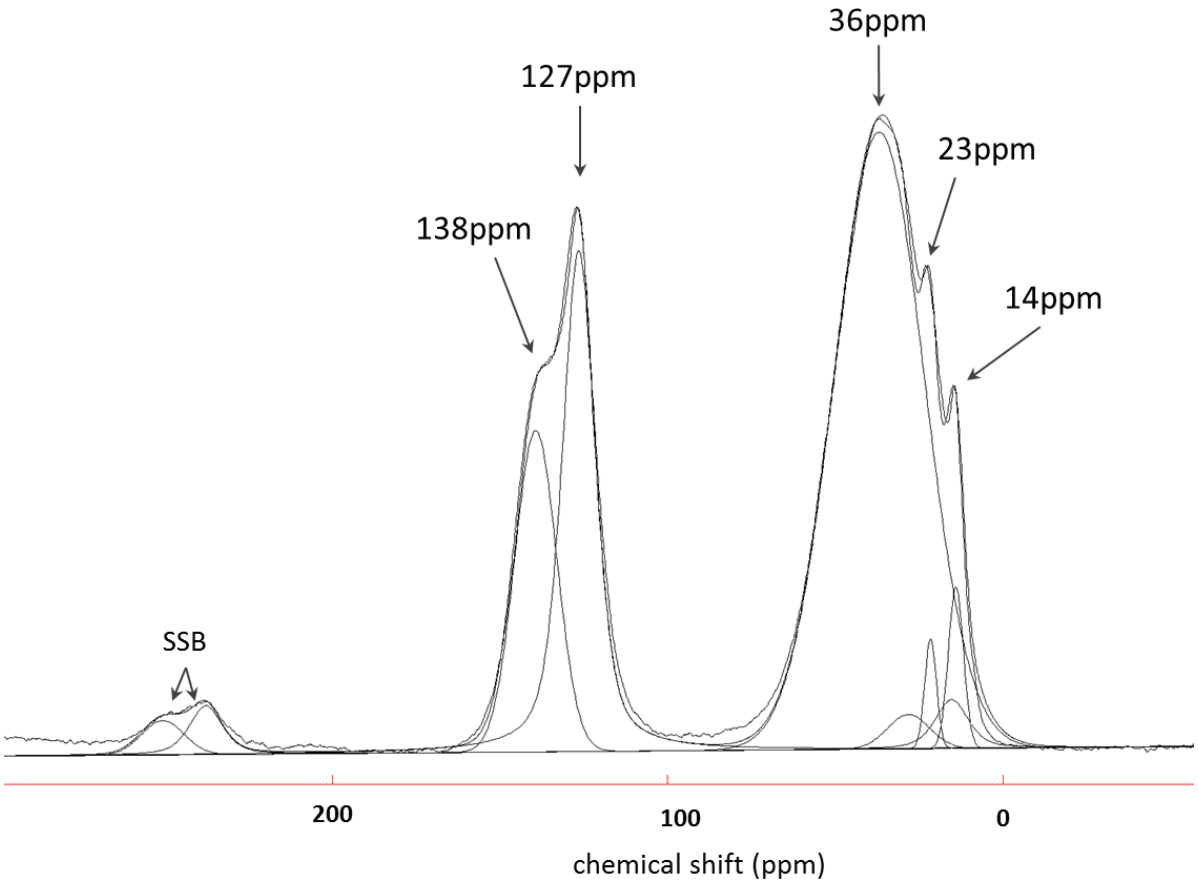
36ppm
127ppm
23ppm
138ppm
14ppm
SSB
200
100
0
chemical shift (ppm)

Fig.5

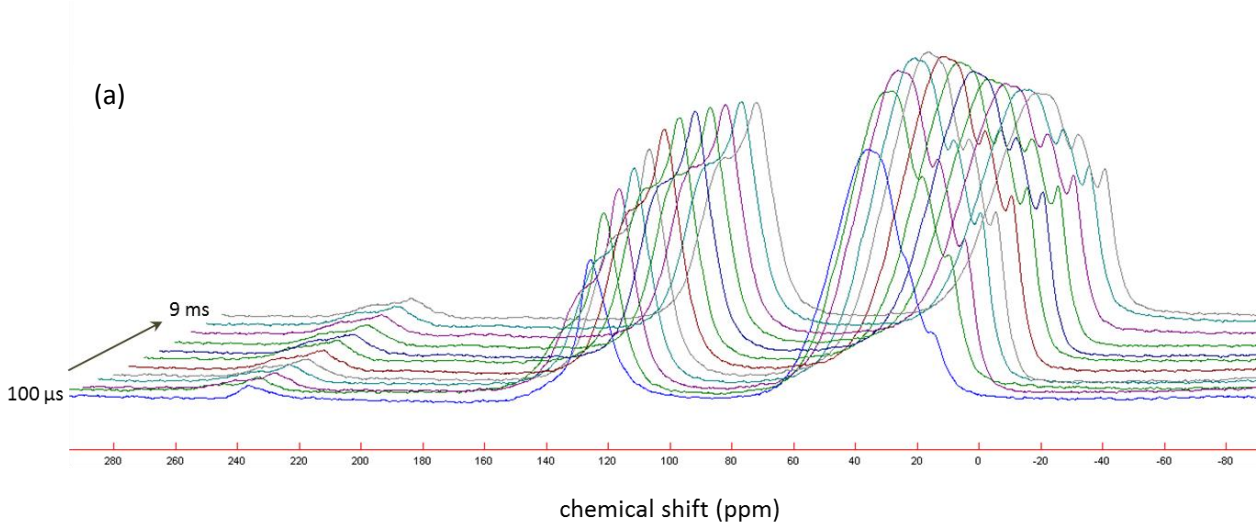
(a)
9 ms
100 µs
280
260
240
220
200
180
160
140
120
100
80
60
40
20
0
-20
-40
-60
-80
chemical shift (ppm)

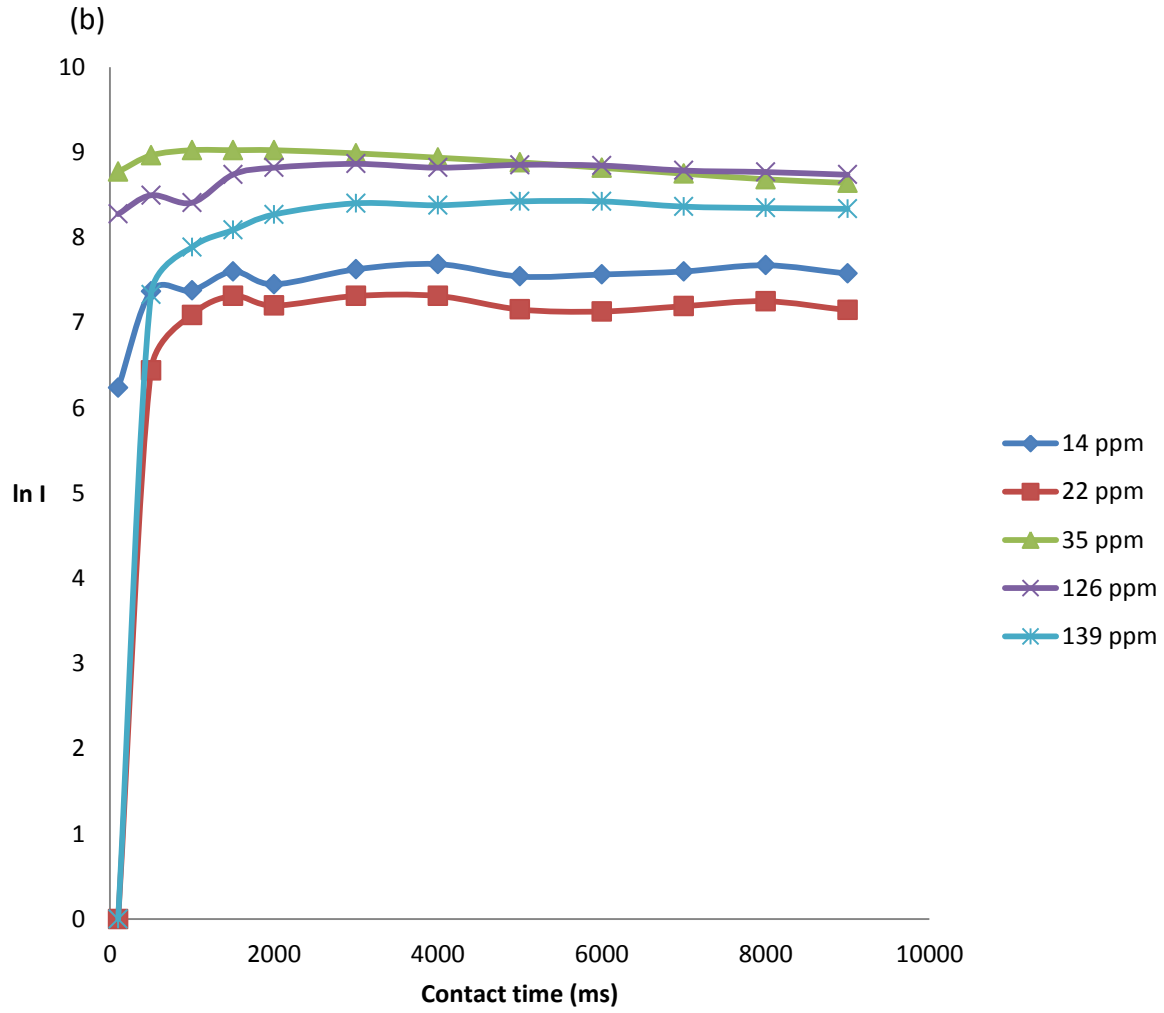
(b)
10
9
8
7
6
5
4
3
2
1
0
ln I
0
2000
4000
6000
8000
10000
Contact time (ms)
14 ppm
22 ppm
35 ppm
126 ppm
139 ppm

Fig. 6

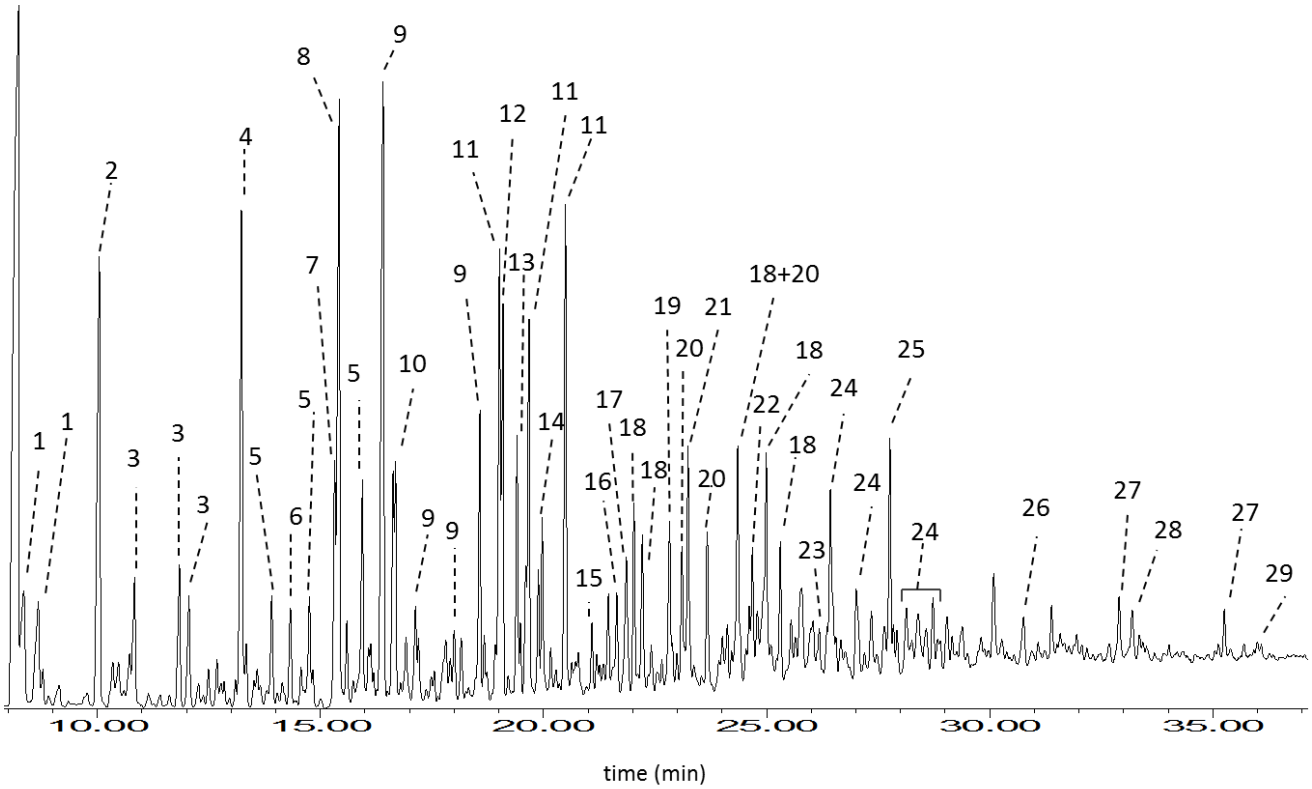

Fig. 7

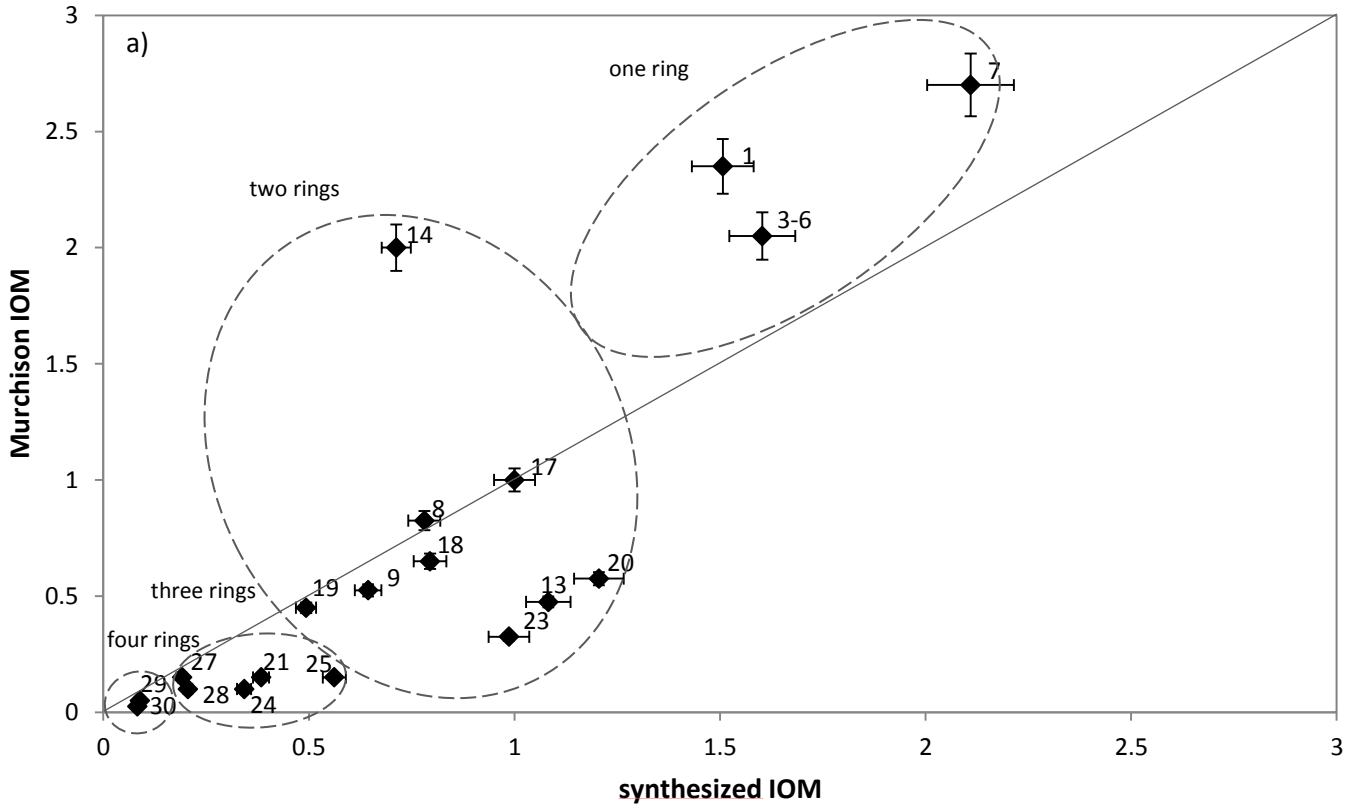
a)
one ring
two rings
three rings
four rings
7
1
3-6
14
17
8
18
20
19
9
13
23
27
21
25
29
28
24
30
Murchison IOM
synthesized IOM
0
0.5
1
1.5
2
2.5
3

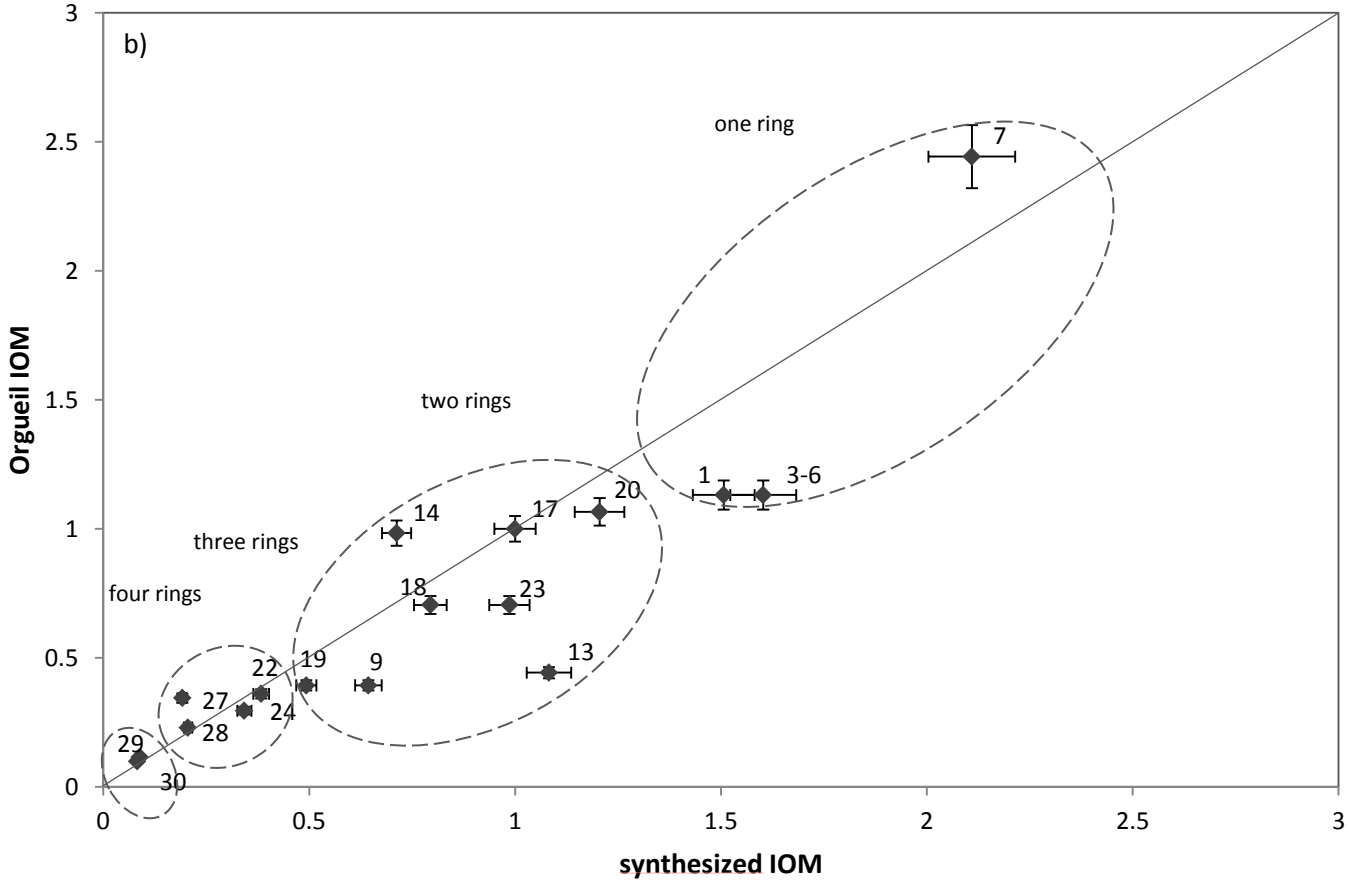
b)
one ring
two rings
three rings
four rings
7
1
3-6
20
14
17
18
23
13
19
9
22
27
24
28
29
30
Orgueil IOM
synthesized IOM
0
0.5
1
1.5
2
2.5
3

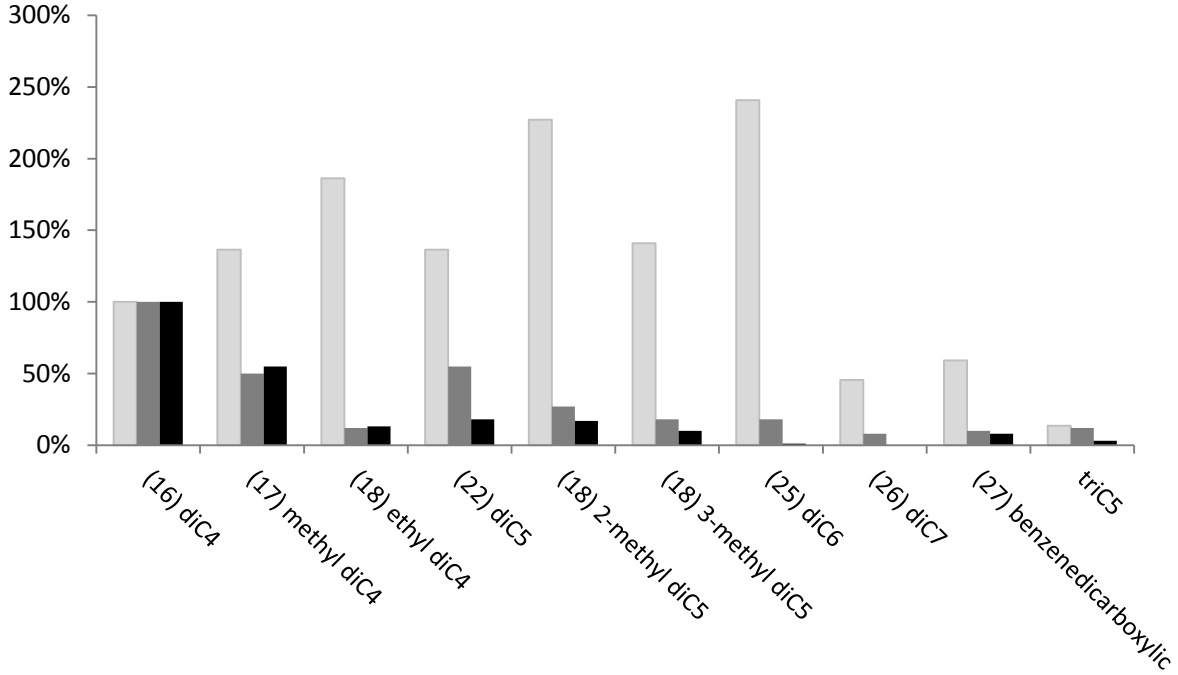
300%
250%
200%
150%
100%
50%
0%
(16) diC4
(17) methyl diC4
(18) ethyl diC4
(22) diC5
(18) 2-methyl diC5
(18) 3-methyl diC5
(25) diC6
(26) diC7
(27) benzenedicarboxylic
triC5

Fig. 9